23p

N63-15031

Code-1

Technical Report No. 32-366

The Laminar Boundary Layer on a Disk of Finite Radius in a Rotating Flow. Part II: A Simplified Momentum-Integral Method

Leslie M. Mack

jpl
JET PROPULSION LABORATORY
CALIFORNIA INSTITUTE OF TECHNOLOGY
PASADENA, CALIFORNIA

January 31, 1963

NATIONAL AERONAUTICS AND SPACE ADMINISTRATION
CONTRACT NO. NAS 7-100

Technical Report No. 32-366

The Laminar Boundary Layer on a Disk of Finite Radius in a Rotating Flow. Part II: A Simplified Momentum-Integral Method

Leslie M. Mack

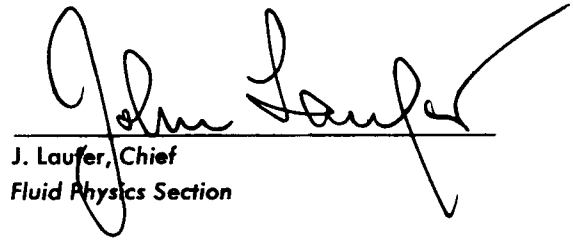

J. Laufer, Chief
Fluid Physics Section

JET PROPULSION LABORATORY
CALIFORNIA INSTITUTE OF TECHNOLOGY
PASADENA, CALIFORNIA

January 31, 1963

CONTENTS

FIGURES

Page intentionally left blank

FIGURES (Cont'd)

ABSTRACT

5031

The momentum-integral method used previously in the study of the laminar boundary layer in a rotating flow is simplified by applying the radial compatibility condition to eliminate one of the two unknowns. It is possible, as a result, to satisfy only a single momentum equation, and the one selected is the tangential momentum equation. The solution of the radial momentum equation is discarded because it fails to give the correct radial mass-flow distribution for the free-vortex outer flow. The solution of the tangential momentum equation is applied to the power-law outer flows treated in Part I of this Report, and also to the outer flows having the tangential velocity distribution of Burgers' vortex. The latter flow contains features of an actual outer flow over the entire disk. In contrast to Part I, a physically satisfactory solution is obtained at the center of the disk for the case where the outer flow is in solid-body rotation, and furthermore Stewartson's conjecture that this solution will be the solution for the disk of infinite radius is found to be correct. For the Burgers' vortex, the solution at the center is the infinite-radius solution based on the local angular velocity. It is further found that when the angular velocity at the center of the disk becomes large compared to the angular velocity at the edge, the magnitude of the axial outflow velocity required to discharge the secondary flow from the boundary layer is no longer small compared to the tangential velocity of the outer flow.

I. INTRODUCTION

In Part I of this Report (Ref. 1), the momentum-integral method originally developed by von Kármán (Ref. 2) for the turbulent boundary layer on a rotating disk was used to investigate the problem of the laminar boundary layer on a stationary disk of finite radius in a rotating outer flow. In this method, called the T method in Part I, the radial and tangential velocity profiles are independent of the radius, the radial compatibility condition is not satisfied, and the solution is obtained by numerical integration of the radial and tangential momentum equations.

There were two important points left unsettled in Part I. The first of these concerned the type of radial mass flow distribution when the outer flow is a free vortex. The result given by the T method, first obtained by Taylor (Ref. 3), is that the inward radial mass flow increases monotonically with decreasing radius. A contrary result, obtained with a different method by Cooke (Ref. 4), is that the radial mass flow has a maximum at $r = 0.45$, where r is the radius, and approaches zero as $r \to 0$. The question of which distribution is the correct one has since been answered by the author in Ref. 5, where a six-term series solution of the boundary-layer equations was obtained verifying Taylor's result. Therefore, a necessary requirement for any momentum-integral method is that it produce the Taylor distribution for the free-vortex outer flow.

The second point concerned the behavior of the boundary-layer solution at $r = 0$, for the case where the outer flow is in solid-body rotation. Stewartson (Ref. 6) has conjectured that Bödewadt's solution (Ref. 7) for the disk of infinite radius should be obtained at $r = 0$. The T method does indeed produce the momentum-integral solution of Bödewadt's problem at $r = 0$, at least for certain boundary-layer velocity profiles, but it also gives, at $r = 0$, infinite derivatives with respect to r of the boundary-layer thickness and the axial outflow velocity. This difficulty is related to the assumed velocity profiles. The tangential velocity in Bödewadt's solution overshoots the outer flow value by 25% and then oscillates about it with decreasing amplitude. As a result, the integral through the boundary layer of $1 - g^2$, where g is the tangential-velocity profile function, is negative, whereas for the monotonic profiles used in Part I the integral is necessarily positive. It is only with a negative integral that zero derivatives can be obtained at $r = 0$ with the T method; however, then the solution near $r = 1$ can no longer be obtained.

It was suggested in Part I that a method used by Cochran (Ref. 8) for the rotating-disk problem, in which the tangential-velocity profiles are a one-parameter family, be investigated for the stationary-disk problem. The author applied this method to Bödewadt's problem and found that a velocity profile with an overshoot was indeed obtained. However, since the integral of $1 - g^2$ was still positive, the method was abandoned.

It was also pointed out in Part I that a satisfactory boundary-layer solution could perhaps be obtained by applying the radial compatibility condition to eliminate one of the two unknowns of the T method, and then solving only one of the two momentum equations. This approach is investigated here in Part II. Approximate solutions are obtained from the radial momentum equation alone plus the radial compatibility condition, and from the tangential momentum equation alone plus the radial compatibility condition. The first of these solutions is found to give a radial mass-flow distribution of the Cooke type for the free vortex case and is therefore unsatisfactory, but the second solution gives the correct distribution. Near the center of the disk, with the outer flow in solid-body rotation, the solution of the tangential momentum equation gives not only the Bödewadt solution, but also, since the integral of $1 - g^2$ occurs only in the radial momentum equation, the desired zero derivatives for all velocity profiles.

In view of the success of the solution of the tangential momentum equation in treating the flow near $r = 0$ for the solid-body outer flow, the solution is also applied in this Report to an outer flow which has two essential features of an actual tangential velocity distribution over the entire disk. These two features are that the tangential velocity has a maximum at a radius greater than zero, and that the tangential velocity is locally a solid-body rotation in the immediate vicinity of $r = 0$. Burgers' vortex (Ref. 9), which is a free vortex far from $r = 0$ and a solid-body rotation near $r = 0$, is chosen to represent this type of outer flow. It cannot be an actual outer flow because the axial velocity is independent of r and, therefore, incompatible with the axial outflow velocity of the boundary layer solution. The extension, suggested in Part I, of Stewartson's conjecture is found to be true for this outer flow and for any outer flow that is locally a solid-body rotation at $r = 0$. That is, the solution at $r = 0$ is simply Bödewadt's solution based on the local angular velocity.

II. DERIVATION OF APPROXIMATE SOLUTIONS

A. General Analysis

From Part I, the dimensionless boundary-layer momentum equations, in cylindrical coordinates and with axial symmetry, are

$$u\frac{\partial u}{\partial r} + w\frac{\partial u}{\partial z} - \frac{v^2}{r} = -\frac{v_\infty{}^2}{r} + \frac{\partial^2 u}{\partial z^2} \tag{2-1}$$

$$u\frac{\partial v}{\partial r} + w\frac{\partial v}{\partial z} + \frac{uv}{r} = \frac{\partial^2 v}{\partial z^2} \tag{2-2}$$

where r is the radius, z the axial coordinate, u, v, and w the radial, tangential and axial velocities, respectively, and v_∞ the specified tangential velocity of the outer flow. The definitions of the dimensionless quantities are

$$u = \frac{u^*}{v_1{}^*} \qquad v = \frac{v^*}{v_1{}^*} \qquad w = \frac{w^*}{v_1{}^*}(\mathrm{Re}_t)^{1/2}$$
$$r = \frac{r^*}{r_1{}^*} \qquad z = \frac{z^*}{r_1{}^*}(\mathrm{Re}_t)^{1/2} \tag{2-3}$$

The asterisks refer to dimensional quantities; $r_1{}^*$ is the radius of the disk; $v_1{}^*$ is the outer-flow tangential velocity at $r^* = r_1{}^*$; and Re_t is the peripheral tangential Reynolds number defined by

$$\mathrm{Re}_t = \frac{v_1{}^* r_1{}^*}{\nu^*} \tag{2-4}$$

where ν^* is the kinematic viscosity coefficient. The continuity equation is

$$\frac{\partial}{\partial r}(ru) + \frac{\partial}{\partial z}(rw) = 0 \tag{2-5}$$

The momentum-integral equations are obtained by integrating the boundary-layer equations with respect to z and eliminating the axial velocity at the edge of the boundary layer by use of the integrated continuity equation. The resulting equations are

$$\frac{d}{dr}\left(r\int_0^\delta u^2\,dz\right) + \int_0^\delta (v_\infty{}^2 - v^2)\,dz = -r\left(\frac{\partial u}{\partial z}\right)_{z=0} \tag{2-6}$$

$$\frac{d}{dr}\left(r^2\int_0^\delta uv\,dz\right) - rv_\infty\frac{d}{dr}\left(r\int_0^\delta u\,dz\right) = -r^2\left(\frac{\partial v}{\partial z}\right)_{z=0} \tag{2-7}$$

where δ is the value of z at the edge of the boundary layer.

In the T method, which was used for the investigations of Part I, the velocity components are represented by

$$u(r,z) = v_\infty(r)\,E(r)\,f\left(\frac{z}{\delta}\right) \tag{2-8}$$

$$v(r,z) = v_\infty(r)\,g\left(\frac{z}{\delta}\right) \tag{2-9}$$

This representation provides two unknown functions, E and δ, for the two equations (2-6) and (2-7). The present approach uses the radial compatibility condition to reduce the number of unknowns to one, and thereby does away with the need for both momentum equations. The radial compatibility condition

$$\left(\frac{\partial^2 u}{\partial z^2}\right)_{z=0} = \frac{v_\infty{}^2}{r} \tag{2-10}$$

is obtained by evaluating Eq. (2-1) at $z = 0$. When Eq. (2-8) is substituted into Eq. (2-10), E is found to be

$$E = \frac{v_\infty}{r}\frac{\delta^2}{f''(0)} \tag{2-11}$$

where the primes refer to differentiation with respect to the boundary-layer variable η, which is defined by

$$\eta = \frac{z}{\delta} \tag{2-12}$$

Therefore, the expression for the radial velocity becomes

$$u(r,\eta) = \frac{v_\infty{}^2}{r}\delta^2\frac{f(\eta)}{f''(0)} \tag{2-13}$$

B. Solution of Tangential Momentum Equation Only

When Eqs. (2-9) and (2-13) are substituted into the integrated tangential momentum equation, Eq. (2-7), and the two integrals are written in terms of η, the result is

$$\frac{d}{dr}(rv_\infty{}^2\delta^4)\int_0^1 \frac{f(\eta)}{f''(0)}g(\eta)\,d\eta - rv_\infty\frac{d}{dr}(v_\infty{}^2\delta^3)\int_0^1 \frac{f(\eta)}{f''(0)}\,d\eta = -r^2 v_\infty g'(0) \tag{2-14}$$

The two integrals in this equation, which are constants for given radial and tangential velocity profiles, are used to define the following two velocity-profile constants.

$$B = \frac{\int_0^1 f(1-2g)\,d\eta}{\int_0^1 f(1-g)\,d\eta} \tag{2-15}$$

$$D = \frac{g'(0)}{\int_0^1 f(1-g)\,d\eta} \tag{2-16}$$

These constants are identical to two of the four constants that appear in the T-method equations. After some manipulation, the equation can be reduced to the form

$$\frac{d}{dr}(\delta^4 v_\infty^{8/3}) - \frac{4}{3}\delta^4 v_\infty^{8/3}(1-B)\frac{d}{dr}(\log r v_\infty) + r v_\infty^{2/3}\left[-\frac{4}{3}f''(0)D\right] = 0 \tag{2-17}$$

This equation can be immediately integrated to give, with the initial condition $\delta(1) = 0$,

$$\delta^4 = \left[-\frac{4}{3}f''(0)D\right]\frac{r^{8/3}}{\Gamma_\infty^{(4/3)(1+B)}}\int_r^1 \frac{r^{1/3}}{\Gamma_\infty^{(2/3)(1-B)}}\,dr \tag{2-18}$$

where

$$\Gamma_\infty = v_\infty r \tag{2-19}$$

is the dimensionless circulation of the outer flow. Thus, the single-equation method has reduced the boundary-layer problem to the evaluation of an integral.

Before the properties of this solution are examined, the preceding results will be rewritten, as was done in Part I, to take advantage of the existence of a similarity solution of the boundary-layer equations near $r = 1$. The similarity equations and their solution were first given by Stewartson (Ref. 6). A more exact numerical calculation of the solution is included in Part I. From Eq. (2-17) it follows that near $r = 1$

$$\delta^4 = -\frac{4}{3}f''(0)D(1-r) \tag{2-20}$$

This result is the momentum-integral counterpart of the exact similarity solution. It is apparent from Eq. (2-20) that the similarity variable is

$$y = \frac{z}{(1-r)^{1/4}} \tag{2-21}$$

At the edge of the boundary layer, according to Eq. (2-20), the value of y is

$$y_\delta = \frac{\delta}{(1-r)^{1/4}} = \left[-\frac{4}{3}f''(0)D\right]^{1/4} \tag{2-22}$$

The radial velocity near $r = 1$ is, from Eqs. (2-13), (2-20), and (2-22)

$$u = (y_\delta)^2\frac{f(\eta)}{f''(0)}(1-r)^{1/2} \tag{2-23}$$

or, in terms of a similarity radial-velocity profile function, $\tilde{f}(y)$,

$$u = -\tilde{f}(y)(1-r)^{1/2} \tag{2-24}$$

where

$$\tilde{f}(y) = -(y_\delta)^2\frac{f(\eta)}{f''(0)} \tag{2-25}$$

In the similarity region, $\eta = y/y_\delta$. The similarity tangential-velocity profile function is

$$\tilde{g}(y) = g(\eta) \tag{2-26}$$

When the exact, or Stewartson, velocity profiles are used in the momentum-integral method, $\tilde{f}(y)$ and $\tilde{g}(y)$ are given directly by the exact solutions of the boundary-layer equations in the similarity region, and Eqs. (2-25) and (2-26) do not apply. However, when polynomial velocity profiles are used, these two equations provide the proper normalization so that $\tilde{f}$ and $\tilde{g}$ satisfy the same integrated equations as the exact solutions.

When the velocity-profile constant B is written in terms of $\tilde{f}$ and $\tilde{g}$ instead of f and g, and with y as the variable of integration instead of η, the result is

$$B = \frac{\int_0^{y_\delta}\tilde{f}(1-2\tilde{g})\,dy}{\int_0^{y_\delta}\tilde{f}(1-\tilde{g})\,dy} \tag{2-27}$$

Therefore, B is unchanged in form except that the upper limit of integration is y_δ instead of 1. However, when these changes are made in Eq. (2-16) for D, the identity

$$\frac{\tilde{g}'(0)}{\int_0^{y_\delta}\tilde{f}(1-\tilde{g})\,dy} = \frac{3}{4} \tag{2-28}$$

is obtained. Equation (2-28) is simply the integrated form of Stewartson's tangential momentum equation.

With the new dependent variable

$$\tilde{\delta} = \frac{\delta}{y_\delta} \tag{2-29}$$

Eq. (2-17) becomes

$$\frac{d}{dr}(\tilde{\delta}^4 v_\infty^{8/3}) - \frac{4}{3}\tilde{\delta}^4 v_\infty^{8/3}(1-B)\frac{d}{dr}(\log r v_\infty) + r v_\infty^{2/3} = 0 \tag{2-30}$$

and the solution, from Eq. (2-18), is

$$\tilde{\delta}^4 = \frac{r^{8/3}}{\Gamma_\infty^{\frac{4}{3}(1+B)}} \int_r^1 \frac{r^{1/3}}{\Gamma_\infty^{\frac{2}{3}(1-2B)}}\, dr \tag{2-31}$$

Either polynomial velocity profiles or Stewartson's similarity profiles may be used in the preceding equations. The only difference in the results for the two types of profiles is that an actual $\delta(r)$ can be obtained for the polynomial velocity profiles, since D can be computed from Eq. (2-16) and therefore y_δ from Eq. (2-22). However, for the Stewartson profiles all that is obtained is $\tilde{\delta}$, the ratio of δ to whatever y_δ is chosen to represent the edge of the boundary layer. The reason for using the Stewartson profiles is that, just as in Part I, the momentum-integral solution near $r = 1$ is then also the exact solution of the boundary-layer equations.

When $\tilde{\delta}$ has been determined as a function of r, then the other flow quantities can be found. The inward radial mass flow induced in the boundary layer by the radial pressure gradient is

$$M^* = -2\pi\rho^* r^* \int_0^{\delta^*} u^*\, dz^* \tag{2-32}$$

The dimensionless radial mass flow, defined by

$$M = \frac{M^*(\mathrm{Re}_t)^{1/2}}{2\pi\rho^* {r_1^*}^2 v_1^*} \tag{2-33}$$

is, from Eqs. (2-13) and (2-25),

$$M = v_\infty^2 \tilde{\delta}^3 \tilde{I}_1 \tag{2-34}$$

where

$$\tilde{I}_1 = \int_0^\infty \tilde{f}(y)\, dy \tag{2-35}$$

The dimensionless axial outflow velocity, which is the axial velocity as defined in Eq. (2-3) evaluated at the edge of the boundary layer, can be established from the mass-flow balance in the boundary layer to be

$$w_\infty = \frac{1}{r}\frac{dM}{dr} \tag{2-36}$$

From Eqs. (2-34) and (2-30),

$$w_\infty = \left[\frac{\tilde{\delta}^3 v_\infty^2}{r}(1-B)\frac{d}{dr}(\log\Gamma_\infty) - \frac{3}{4}\frac{1}{\tilde{\delta}}\right]\tilde{I}_1 \tag{2-37}$$

This result can also be obtained from the T-method expression for w_∞ in Part I when Eq. (2-11) is used for E.

With the dimensionless shear stress defined by

$$\tau = \frac{\tau^*}{\rho^* {v_1^*}^2}(\mathrm{Re}_t)^{1/2} \tag{2-38}$$

the radial and tangential shear stresses at the surface of the disk are easily found to be

$$\tau_r = \left(\frac{\partial u}{\partial z}\right)_{z=0} = -\tilde{f}'(0)\frac{v_\infty^2\tilde{\delta}}{r} \tag{2-39}$$

and

$$\tau_t = \left(\frac{\partial v}{\partial z}\right)_{z=0} = \tilde{g}'(0)\frac{v_\infty}{\tilde{\delta}} \tag{2-40}$$

where the primes refer to differentiation with respect to y. The dimensionless torque, defined by

$$T = \frac{T^*}{2\pi\rho^* {v_1^*}^2 {r_1^*}^3}(\mathrm{Re}_t)^{1/2} \tag{2-41}$$

is, as in Part I,

$$T(r) = \tilde{g}'(0)\int_r^1 \frac{r^2 v_\infty^2}{\tilde{\delta}}\, dr \tag{2-42}$$

where $T^*(r^*)$ is the torque exerted by the fluid on the portion of the disk between r^* and ${r_1}^*$.

Finally, the angle between the circumferential direction and the direction of the surface streamline is

$$\theta = \tan^{-1}\left[-\frac{v_\infty}{r}\tilde{\delta}^2\frac{\tilde{f}'(0)}{\tilde{g}'(0)}\right] \tag{2-43}$$

The adequacy of the solution of the tangential momentum equation, Eq. (2-31), will now be tested by applying it to the calculation of the radial mass flow distribution for a free-vortex outer flow. For the free vortex, $\Gamma_\infty = 1$, and Eq. (2-31) gives

$$\tilde{\delta}^4 = \frac{3}{4} r^{8/3}(1 - r^{4/3}) \tag{2-44}$$

It follows from Eq. (2-34) that

$$M = \left(\frac{3}{4}\right)^{3/4} \tilde{I}_1 (1 - r^{4/3})^{3/4} \tag{2-45}$$

Consequently, M increases monotonically with decreasing r and has zero slope at $r = 0$. The value of M at $r = 0$ for the Stewartson radial velocity profile, since $\tilde{I}_1 = 1.6915$, is

$$M(0) = 1.363 \tag{2-46}$$

The T method gives the same distribution and the numerical value $M(0) = 1.181$.

The series solution of the boundary-layer equations, which was mentioned in Part I as a means of obtaining a reliable solution to use as a test for the momentum-integral methods, has recently been carried out by the author (Ref. 5). This method was originally suggested by Stewartson (Ref. 6) for the case where the outer flow is in solid-body rotation. It is not, however, well suited to that problem, but is succesful when applied to the case of the free-vortex outer flow. The result for the free-vortex outer flow given by a six-term series is shown in Fig. 1, which also shows the results given by (1) Eq. (2-45), (2) the T method with Stewartson velocity profiles, (3) Garbsch (Ref. 10), and (4) Cooke (Ref. 4). These results all agree with the series solution except Cooke's, which can therefore finally be discarded as incorrect. The fact that Eq. (2-45), although numerically somewhat wide of the mark, gives the correct behavior of M, in spite of its extreme simplicity, encourages further use of the single-equation method.

The result of Garbsch, which was unfortunately overlooked in Part I, deserves some comment. It was obtained by a method in which the solution at a given radius is the similarity solution, written in terms of two special

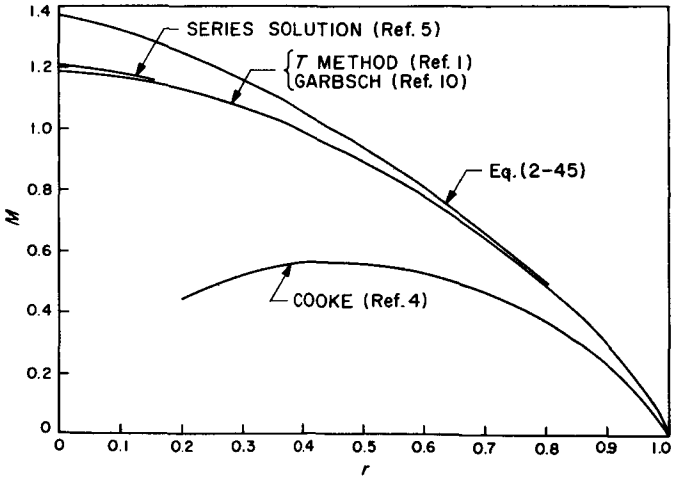

Fig. 1. Comparison of radial mass flow distribution for free-vortex outer flow according to five different methods

functions of r, plus correction terms. When the velocity profiles are close to the similarity profiles, as the series solution shows is the case for the free-vortex outer flow, the correction terms are negligible and the re-interpreted similarity solution, to the accuracy with which Garbsch's small plot can be read, gives a result sufficiently close to the T-method result that a separate curve cannot be drawn in Fig. 1.

C. Solution of Radial Momentum Equation Only

When Eqs. (2-9) and (2-13) are substituted into the radial momentum equation, Eq. (2-6), instead of into the tangential momentum equation, the result is

$$\frac{d}{dr}\left(\frac{\delta^5 v_\infty^4}{r^2}\right)\int_0^1 \left[\frac{f(\eta)}{f'(0)}\right]^2 d\eta + \delta v_\infty^2 \int_0^1 [1 - g^2(\eta)]\, d\eta = -v_\infty^2 \delta \frac{f'(0)}{f'(0)} \tag{2-47}$$

The two integrals in this equation are used to define the following velocity-profile constants:

$$A = \frac{\int_0^1 (1 - g^2)\, d\eta}{\int_0^1 f^2\, d\eta} \tag{2-48}$$

$$C = \frac{f'(0)}{\int_0^1 f^2\, d\eta} \tag{2-49}$$

These constants, as were B and D, are identical to two of the four constants in the T method. Equation (2-47) can now be put in the form

$$\frac{d}{dr}\left(\frac{\delta^4 v_\infty^2}{r^2}\right) + \frac{6}{5}\left(\frac{\delta^4 v_\infty^2}{r^2}\right)\frac{d}{dr}(\log r v_\infty) + \frac{4}{5} f''(0)[f''(0)\, A + C]\frac{1}{r} = 0 \tag{2-50}$$

It follows from this equation that near $r = 1$

$$\delta^4 = \frac{4}{5} f''(0)\, [f''(0)\, A + C]\, (1 - r) \tag{2-51}$$

Consequently the Stewartson similarity variable at the edge of the boundary layer is

$$y_\delta = \frac{4}{5}\left\{f''(0)\, [f''(0)\, A + C]\right\}^{1/4} \tag{2-52}$$

The equation for $\tilde{\delta} = \delta/y_\delta$, which is the counterpart of Eq. (2-30) obtained from the tangential momentum equation, is

$$\frac{d}{dr}\left(\frac{\tilde{\delta}^4 v_\infty{}^2}{r^2}\right) + \frac{6}{5}\left(\frac{\tilde{\delta}^4 v_\infty{}^2}{r^2}\right)\frac{d}{dr}(\log \Gamma_\infty) + \frac{1}{r} = 0 \tag{2-53}$$

where the circulation Γ_∞ has been introduced. The solution of Eq. (2-53) is

$$\tilde{\delta}^4 = \frac{r^4}{\Gamma_\infty{}^{16/5}} \int_r^1 \frac{\Gamma_\infty{}^{6/5}}{r}\, dr \tag{2-54}$$

For the free-vortex outer flow, $\Gamma_\infty = 1$, and Eq. (2-54) gives

$$\tilde{\delta}^4 = -r^4 \log r \tag{2-55}$$

The inward radial mass flow in the boundary layer is still given by Eq. (2-34), with $\tilde{I}_1$ defined by Eq. (2-35) and $\tilde{f}(y)$ by Eq. (2-25) for a polynomial velocity profile. The only difference from the previous formulation is that here y_δ is given by Eq. (2-52) instead of Eq. (2-22). Consequently, the radial mass flow for the free-vortex outer flow, according to the solution of the radial momentum equation, is

$$M = -r(\log r)^{3/4}\tilde{I}_1 \tag{2-56}$$

The noteworthy thing about Eq. (2-56) is that at $r = 0$ it yields $M = 0$. Therefore, M must have a maximum somewhere between $r = 1$ and $r = 0$. From Eq. (2-56) the maximum is found to be located at

$$r_{max} = \frac{1}{e^{3/4}} = 0.4724 \tag{2-57}$$

for all velocity profiles. The value of the maximum mass flow is

$$M_{max} = 0.3807\tilde{I}_1 \tag{2-58}$$

For the Stewartson radial velocity profile, $\tilde{I}_1 = 1.6915$ and $M_{max} = 0.6519$.

The above result agrees with Cooke, and disagrees with the monotonic mass flow distribution given by the series solution, T method, tangential momentum equation, and by Garbsch. Cooke used the same radial velocity profile as Taylor, $u = \eta(1 - \eta)^2$, but his tangential velocity profile, which satisfies the tangential compatibility condition, was $v = (1/2)(3 - \eta^2)$. The values of the profile constants A, C, and I_1 for these profiles are 54, 105, and 1/12. From Eq. (2-52), $y_\delta = 4.341$, and from Eqs. (2-25) and (2-35), $\tilde{I}_1 = 1.705$. Therefore, according to Eq. (2-58), $M_{max} = 0.649$. Cooke's values are $r_{max} = 0.45$ and $M_{max} = 0.56$. With Taylor's tangential velocity profile, $v = \eta(2 - \eta)$, Eq. (2-58) gives $M_{max} = 0.559$.

The solution of the radial momentum equation will be abandoned at this point because it fails to give the well-established distribution of the radial mass flow for the free-vortex outer flow. All further work in this report will use the solution of the tangential momentum equation.

III. APPLICATIONS OF THE SOLUTION OF THE TANGENTIAL MOMENTUM EQUATION

With an analytic solution of the boundary-layer equations, it is possible to determine the behavior of the boundary layer without having to perform the extensive numerical integrations of Part I. Two types of outer-flow tangential velocity distributions will be considered in this Section. The first type is the power-law distribution, $v_\infty = 1/r^n$, which is found experimentally in vortex chambers and other rotating flows, and which was investigated in considerable detail in Part I by the T method. This velocity distribution, except for $n = -1$, is not applicable near the axis, where the flow must be a solid-body rotation. Therefore, in order to have a distribution which covers the whole region from $r = 1$ to $r = 0$, Burgers' vortex (Ref. 9) is chosen as the second type of velocity distribution. The Burgers' vortex, an exact solution of the Navier-Stokes equations, approaches a free vortex as $r \to \infty$, and a solid-body rotation as $r \to 0$. Since its axial velocity is independent of r and therefore incompatible with the boundary-layer solution, it does not represent an actual outer flow. However, it does contain the essential feature of a transition from a vortex-like flow away from the axis to a solid-body flow near the axis.

A. Power-Law Outer Flow

With

$$v_\infty = \frac{1}{r^n} \tag{3-1}$$

the integral in Eq. (2-31) can be immediately evaluated to yield

$$\tilde{\delta}^4 = \frac{r^{\frac{4}{3}(1+n)-\frac{4}{3}B(1-n)} - r^{2(1+n)}}{\frac{2}{3}(1+n)+\frac{4}{3}B(1-n)} \tag{3-2}$$

When $n = 1$, Eq. (3-2) reduces to Eq. (2-44). The behavior of $\tilde{\delta}$ as a function of r can be seen by inspection of Eq. (3-2). At $r = 0$, for $-1 \leq B < 0$

$$\begin{aligned} &\tilde{\delta} = 0 && \text{for} \quad n > -1 \\ &\tilde{\delta} = -\frac{3}{8B} && n = -1 \\ &\tilde{\delta} \to \infty && n < -1 \end{aligned} \tag{3-3}$$

If $B < -1$, then for $n > 1$ the additional case exists that $\tilde{\delta} \to \infty$ for $n > -(1-B)/(1+B)$. This behavior is in accord with the T-method numerical results except for $n = 1$ and $n > 1$ where, according to the T method, $\tilde{\delta}(0) = \text{const.}$ and $\tilde{\delta}(0) \to \infty$, respectively.

The inward radial mass flow is, from Eqs. (2-34) and (3-2),

$$M = \left(\frac{3}{2}\right)^{\frac{3}{4}} \left[\frac{r^{\frac{4}{3}(1-n)(1-B)} - r^{\frac{2}{3}(3-n)}}{(1+n)+2B(1-n)}\right]^{\frac{3}{4}} \tilde{I}_1 \tag{3-4}$$

Near $r = 0$, Eq. (3-4) gives

$$\begin{aligned} &M \to \infty && \text{for} \quad n > 1 \\ &M = \left(\frac{3}{4}\right)^{\frac{3}{4}} \tilde{I}_1 && n = 1 \\ &M = 0 && n < 1 \end{aligned} \tag{3-5}$$

This behavior is in complete accord with the T-method results. A numerical comparison[1] is given in Fig. 2 for the Stewartson velocity profiles. The location of the maximum radial mass flow, r_{max}, can be found from Eq. (3-4) to be

$$r_{max} = \left[2(1-B)\left(\frac{1-n}{3-n}\right)\right]^{\frac{1}{\frac{2}{3}(1+n)+\frac{4}{3}B(1-n)}} \qquad n \neq \frac{1+2B}{2B-1} \tag{3-6}$$

The axial outflow velocity is, from Eqs. (2-36) and (3-4),

$$w_\infty = \frac{1}{2}\frac{M}{r^2} \times \left[\frac{2(1-n)(1-B)\, r^{\frac{4}{3}(1-n)(1-B)} - (3-n)\, r^{\frac{2}{3}(3-n)}}{r^{\frac{4}{3}(1-n)(1-B)} - r^{\frac{2}{3}(3-n)}}\right] \tag{3-7}$$

An alternate form of w_∞, in terms of r_{max}, is

$$w_\infty = \frac{1}{2}(3-n)\frac{M}{r^2}\left[\frac{1-\left(\frac{r}{r_{max}}\right)^{-\frac{2}{3}(1+n)-\frac{4}{3}B(1-n)}}{1-r^{-\frac{2}{3}(1+n)-\frac{4}{3}B(1-n)}}\right] \tag{3-8}$$

[1]For convenience, all of the numerical results in this Report were obtained by numerical integration of the tangential momentum equation rather than by evaluation of the integral for δ or by use of the analytic formulas. The author wishes to express his thanks to Maxine Linde for writing the IBM 7090 program.

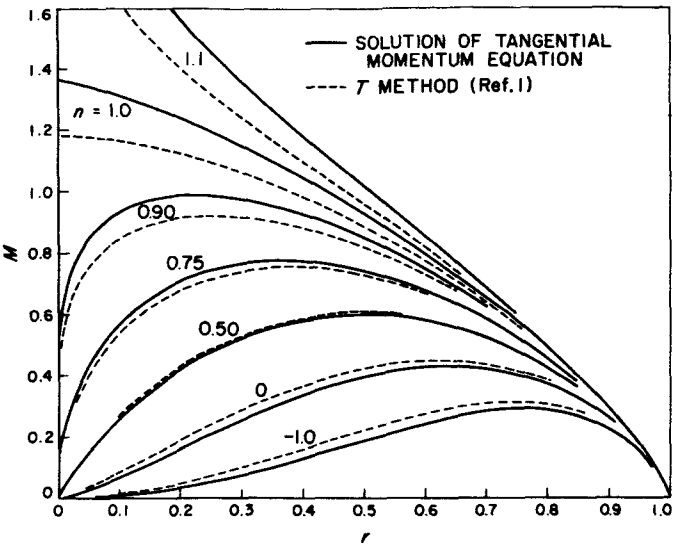

Fig. 2. Radial mass flow distribution for power-law outer flow according to solution of tangential momentum equation and T method

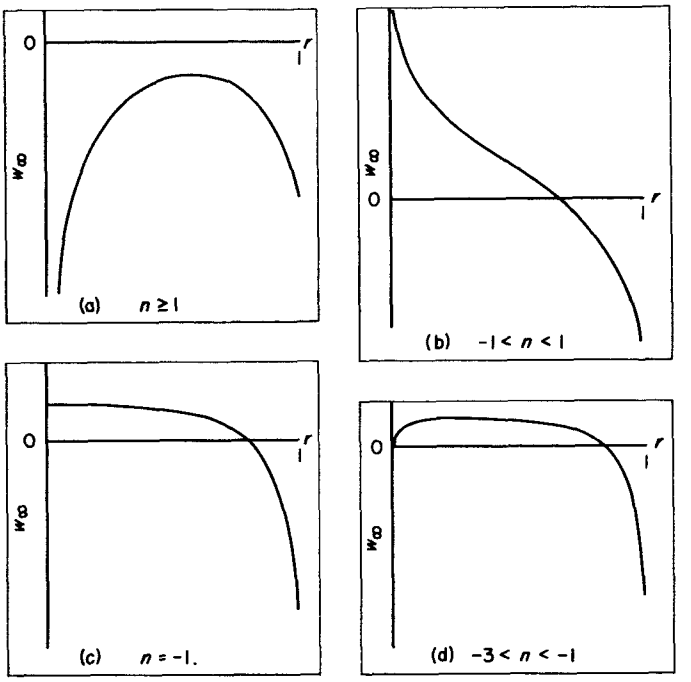

Fig. 3. Schematic representation of axial outflow velocity distribution for power-law outer flow

Therefore, w_∞ is always $-\infty$ at $r = 1$. For $n < 1$, it is negative when $r > r_{max}$ and is positive when $r < r_{max}$. At $r = 0$,

$$
\begin{aligned}
&w_\infty \to -\infty && \text{for} \quad n \geq 1 && \text{(a)}\\
&w_\infty \to \infty && -1 < n < 1 && \text{(b)}\\
&w_\infty = 2\tilde{I}_1\left(-\frac{3}{8B}\right)^{3/4} && n = -1 && \text{(c)}\\
&w_\infty = 0 && n < -1 && \text{(d)}
\end{aligned}
\qquad (3\text{-}9)
$$

Figure 3 shows schematically the complete distribution of w_∞ for each of the above four cases. Of these four cases, only (b) is in complete agreement with the T-method results. The disagreements are in the behavior near $r = 0$. For $n = 1$, the T method gives $w_\infty(0) =$ const., instead of the result shown in Fig. 3. Unfortunately, the series method breaks down as $r \to 0$ and cannot definitely establish the correct $w_\infty(0)$. However, the T-method result is believed to be the correct one. The results of case (d) agree in giving $w_\infty(0) = 0$ but disagree on the behavior of dw_∞/dr as a function of n. Case (c) is of sufficient importance to warrant a separate discussion.

The importance of the boundary-layer solution for the case where the outer flow is in solid-body rotation lies in the fact that any real outer flow is locally of the solid-body type near $r = 0$. Consequently, the solution near $r = 0$ will be related to the solution where the solid-body flow extends over the entire disk. Stewartson (Ref. 6) has conjectured that in the latter case the effect of the edge will be felt over the entire disk except near the center where the Bödewadt similarity solution (Ref. 7) for the disk of infinite radius will be realized. For Stewartson or high-degree polynomial velocity profiles, the T method does indeed produce the momentum-integral Bödewadt solution at $r = 0$. However, the Bödewadt values are attained only by means of physically unsatisfactory infinite derivatives. As case (c) of Fig. 3 shows, the single-equation method yields a w_∞ which, near $r = 0$, has a more satisfactory behavior. In order to demonstrate that the value of w_∞ at $r = 0$ is the Bödewadt value according to the single-equation method, the present solution for $n = -1$ will be discussed in more detail.

Equation (3-2) gives, for $n = -1$,

$$\tilde{\delta}^4 = -\frac{3}{8B}\left(1 - r^{-\frac{8B}{3}}\right) \qquad (3\text{-}10)$$

In contrast to the free-vortex outer flow, this result depends on the assumed velocity profiles. The radial mass flow is, from Eq. (3-4),

$$M = \left(-\frac{3}{8B}\right)^{3/4}\tilde{I}_1\left(1 - r^{-\frac{8B}{3}}\right)^{3/4} r^2 \qquad (3\text{-}11)$$

and the axial outflow velocity is, from Eq. (3-7),

$$w_\infty = 2\left(-\frac{3}{8B}\right)^{3/4}\tilde{I}_1\left(1-r^{-\frac{8B}{3}}\right)^{3/4}\left[1+\frac{Br^{-\frac{8B}{3}}}{1-r^{-\frac{8B}{3}}}\right] \tag{3-12}$$

It can be seen from this equation that $dw_\infty/dr = 0$ at $r = 0$. The maximum radial mass flow, which is located at

$$r_{max} = \left(\frac{1}{1-B}\right)^{-\frac{3}{8B}} \tag{3-13}$$

has the value

$$M_{max} = \left(-\frac{3}{8B}\right)^{3/4}\tilde{I}_1\left(\frac{B}{1-B}\right)^{3/4}\left(\frac{1}{1-B}\right)^{-\frac{3}{4B}} \tag{3-14}$$

For the Stewartson velocity profiles, $r_{max} = 0.764$ and $M_{max} = 0.294$, in reasonable agreement with the corresponding T-method results of $r_{max} = 0.740$ and $M_{max} = 0.316$.

The Bödewadt values, according to the present method, follow directly from Eq. (2-30) with $v_\infty = r$. The similarity solution which is independent of r can only be $\tilde{\delta} = \tilde{\delta}_B = \text{const}$. Therefore

$$\tilde{\delta}_B = \left(-\frac{3}{8B}\right)^{1/4} \tag{3-15}$$

From Eq. (2-34)

$$M_B = \left(-\frac{3}{8B}\right)^{3/4}\tilde{I}_1 r^2 \tag{3-16}$$

and from Eq. (2-36)

$$(w_\infty)_B = 2\left(-\frac{3}{8B}\right)^{3/4}\tilde{I}_1 \tag{3-17}$$

These results are just those given by Eqs. (3-10), (3-11) and (3-12) at $r = 0$. Consequently, within the framework of the present method, Stewartson's conjecture has been proven.

The numerical values of the Bödewadt quantities, for the Stewartson velocity profiles, are

$$\begin{aligned}\tilde{\delta}_B &= 0.8070\\ M_B &= 0.8889\,r^2\\ (w_\infty)_B &= 1.778\end{aligned} \tag{3-18}$$

The exact value of $(w_\infty)_B$ is 1.35, which compares more favorably with the above value than with the T-method value of 3.53.

If the exact Bödewadt velocity profiles are used in the momentum-integral solution of Bödewadt's problem, the exact value of $(w_\infty)_B$ will of course be obtained. In Part I, the Bödewadt profiles were used in the T method in an attempt to get rid of the infinite derivatives at $r = 0$ which were obtained with the Stewartson and polynomial profiles. However, for the Bödewadt profiles, the integral through the boundary layer of $1 - g^2$ and, therefore, the constant A (Eq. 2-48) are negative, and no momentum-integral solution exists in the Stewartson similarity region. The only way a finite-radius solution could be produced was to introduce non-zero initial conditions for δ and E. It was then found that, with $A < 0$, $r = 0$ became a saddle point, and for each value of $\delta(1)$ there was only one value of $E(1)$ for which the integral curve reached $r = 0$. This integral curve had the desired zero derivatives at $r = 0$, but there was no way of proving it to be related to the correct solution for the finite-radius disk with zero initial conditions.

None of these difficulties appear in the present method, since the profile-constant A is absent from the tangential momentum equation. As a result, the behavior of the solution depends only on B, which is negative for all ordinary velocity profiles, including the Bödewadt profiles. Consequently, use of the Bödewadt profiles will only change the numerical values, not the behavior of the solution.

In order to use the Bödewadt radial and tangential velocity profiles, $\bar{f}(z)$ and $\bar{g}(z)$, and avoid the vexing problem of having to assign a boundary-layer thickness to an oscillating profile, the solution will be put into a "Bödewadt" form, just as was done in Part I. From Eq. (2-17),

$$\delta_B{}^4 = \left(-\frac{3}{8B}\right)\left[-\frac{4}{3}f''(0)D\right] \tag{3-19}$$

With the definition

$$\delta = \frac{\delta}{\delta_B} \tag{3-20}$$

Eq. (2-17) becomes

$$\frac{d}{dr}\left(\bar{\delta}^4 v_\infty{}^{8/3}\right) - \frac{4}{3}\bar{\delta}^4 v_\infty{}^{8/3}(1-B)\frac{d}{dr}(\log r v_\infty) + \left(-\frac{8B}{3}\right) r v_\infty{}^{2/3} = 0 \tag{3-21}$$

The constant B is computed from Eq. (2-27) with the tildes replaced by bars, and y by z. If Eq. (3-21) is divided through by $-8B/3$ it is identical to Eq. (2-30) for $\tilde{\delta}$

Therefore, from Eq. (2-31),

$$\bar{\delta}^4 = \left(-\frac{8B}{3}\right)\frac{r^{8/3}}{\Gamma_\infty\,\frac{4}{3}(1+B)}\int_r^1 \frac{r^{1/3}}{\Gamma_\infty\,\frac{2}{3}(1-2B)}\,dr \tag{3-22}$$

For $v_\infty = r$,

$$\bar{\delta}^4 = 1 - r^{-\frac{8B}{3}} \tag{3-23}$$

An expression is needed for the radial mass flow in terms of $\bar{I}_1$,

where

$$\bar{I}_1 = \int_0^\infty \bar{f}(z)dz \tag{3-24}$$

Application of Eq. (2-13) to the Bödewadt similarity region gives

$$u = r(\delta_B)^2\frac{f(\eta)}{f''(0)} = -r\bar{f}(z) \tag{3-25}$$

Therefore,

$$f(\eta) = -\frac{1}{(\delta_B)^2}f''(0)\,\bar{f}(z) \tag{3-26}$$

From the definition of $\tilde{I}_1$ in Eq. (2-35), and with Eqs. (2-25), (2-22), and (3-19), it is found that

$$\tilde{I}_1 = \left(-\frac{8B}{3}\right)^{3/4}\bar{I}_1 \tag{3-27}$$

Equation (2-34) becomes

$$M = v_\infty{}^2\bar{\delta}^3\bar{I}_1 \tag{3-28}$$

a result that could have been obtained more directly.

The numerical values of B and $\bar{I}_1$ for the Bödewadt velocity profiles[2] are

$$B = -2.68 \qquad \bar{I}_1 = 0.675 \tag{3-29}$$

Equation (3-27) gives $\tilde{I}_1 = 2.95$ compared to the Stewartson-profile value of 1.692. For $v_\infty = r$, from Eqs. (3-13) and (3-14), $r_{max} = 0.833$ and $M_{max} = 0.369$, compared to the Stewartson-profile values of $r_{max} = 0.764$ and $M_{max} = 0.294$. Of course, $\bar{\delta}(0) = 1$ and $w_\infty(0)$ equals 1.35, the exact Bödewadt value. In Fig. 4, the distribution of the radial mass flow is shown for both the Stewartson and Bödewadt velocity profiles, along with the distribution for the infinite-radius disk from the exact Bödewadt solution. The corresponding axial outflow velocities are shown in Fig. 5. It is to be noted that with the Bödewadt velocity profiles, the finite-radius solution coincides with the infinite-radius solution as far from the center as $r = \frac{1}{2}$. The exact solution for the disk of finite radius can be expected to start out having values along the distribution obtained with the Stewartson profiles and then as r decreases, to shift gradually over to the distribution obtained with the Bödewadt profiles. This behavior is a reflection of the change of the boundary-layer velocity profiles from the Stewartson profiles at $r = 1$ to the Bödewadt profiles at $r = 0$.

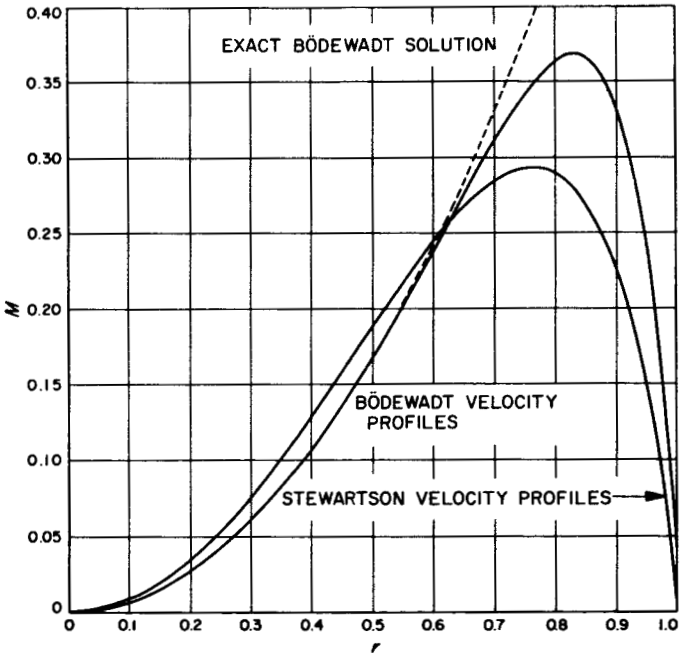

Fig. 4. Radial mass flow distribution for solid-body outer flow. Solution of tangential momentum equation with Stewartson and Bödewadt velocity profiles and exact Bödewadt solution for disk of infinite radius

B. Burgers' Vortex Outer Flow

The tangential velocity of the Burgers' vortex is given by

$$v_\infty = \frac{1}{r}\frac{1-\exp\left[-(1/2)\mathrm{Re}_r r^2\right]}{1-\exp\left[-(1/2)\mathrm{Re}_r\right]} \tag{3-30}$$

where Re_r is a radial Reynolds number. It is to be regarded here simply as a parameter, and is unrelated to the

[2]A recomputation of the solution of Bödewadt's equations on the IBM 7090 with a program which carried 18 decimal digits has shown that Bödewadt's original computation is correct. Consequently, Browning's computation (Ref. 11) is considerably in error, and even that of Rogers and Lance (Ref. 12) is slightly in error (1% in w_∞). An indication of the numerical difficulties involved in the computation is that even with 18 digits only three place accuracy for w_∞ could be obtained by purely numerical means.

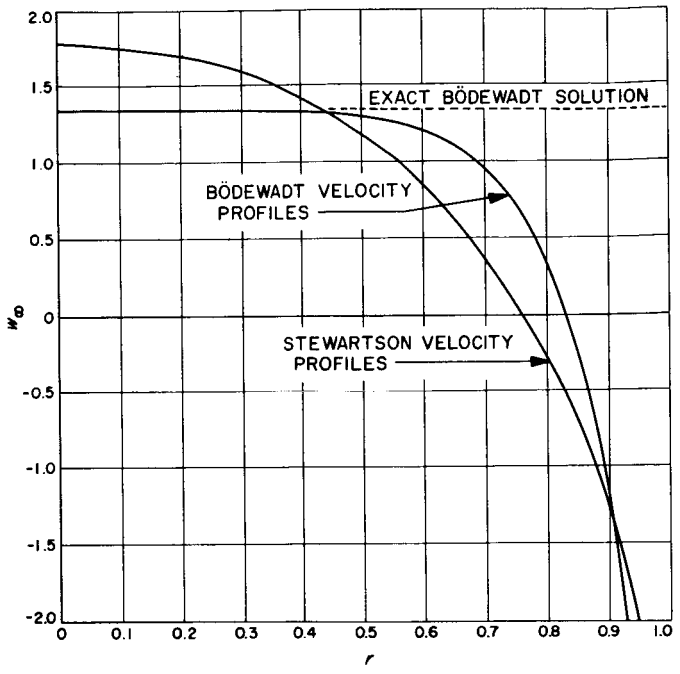

Fig. 5. Axial outflow velocity distribution for solid-body outer flow. Solution of tangential momentum equation with Stewartson and Bödewadt velocity profiles and exact Bödewadt solution for disk of infinite radius

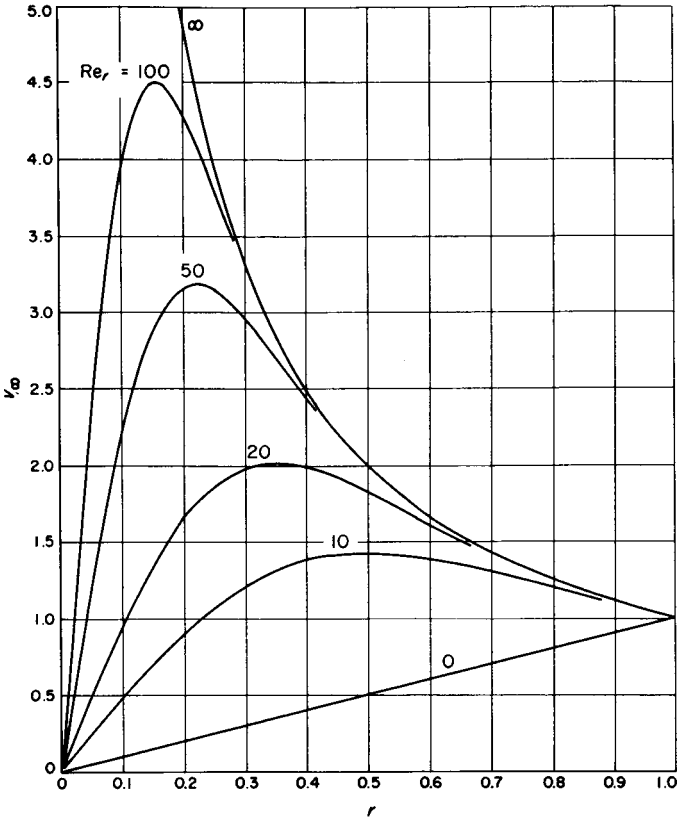

Fig. 6. Tangential velocity distribution of Burgers' vortex

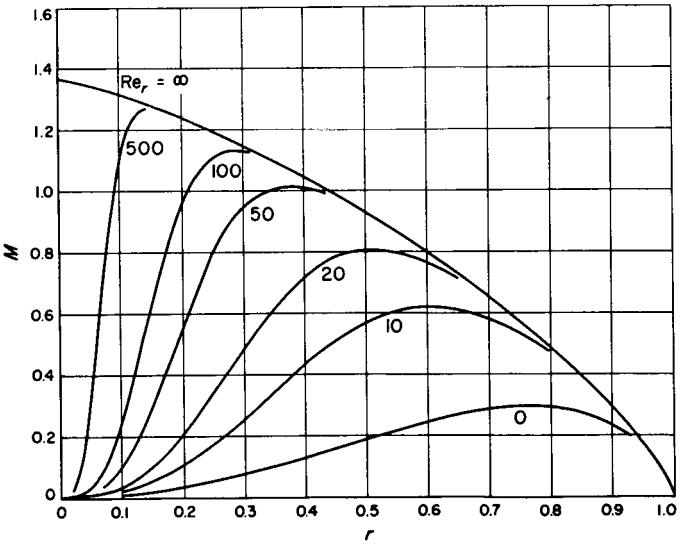

Fig. 7. Radial mass flow distribution for Burgers'-vortex outer flow. Stewartson velocity profiles

radial Reynolds number of an actual outer flow. For larger Re_r, the flow is a free vortex except near the axis, where it is a solid-body rotation with an angular velocity equal to $Re_r/2$. For small Re_r, the flow approaches solid-body rotation for all r. The velocity distributions for several values of Re_r are shown in Fig. 6. The measured tangential velocity distributions in vortex chambers, although of a different type in that they follow power laws with $n < 1$, have maximum velocities which correspond to high values of Re_r. For instance, a typical maximum v_∞ from the experiments of Keyes (Ref. 13) is about 4, a value which is only attained in the Burgers' vortex with $Re_r = 80$.

Since the Stewartson similarity solution at $r = 1$ is independent of the tangential velocity distribution of the outer flow, it is just as suitable for the velocity profiles in the present case as in the case of the power-law outer flow. The distribution of the radial mass flow, as computed from Eqs. (2-31) and (2-34) with the Stewartson velocity-profile constants and Eq. (3-30) for v_∞, is shown in Fig. 7 for several values of Re_r. For $Re_r = 0$, the outer flow is solid-body rotation over the whole disk, and the radial mass flow distribution is identical to the result in Fig. 2 for $n = -1$. As Re_r increases, the free-vortex radial mass flow distribution is followed to smaller and smaller radii, until in the limit as $Re_r \to \infty$ the free-vortex distribution is obtained over the whole disk. For a given Re_r, the maximum radial mass flow occurs at a radius

larger than the radius of maximum v_∞. For Re_r of 50 and larger, the mass flow maximum is located close to the radius at which v_∞ first departs from the free-vortex velocity distribution.

The distribution of the axial outflow velocity for the Burgers' vortex is shown in Fig. 8 for a few Re_r. The usual inflow exists near the edge of the disk, with a subsequent outflow for all radii less than the radius of maximum mass flow. The value of w_∞ at $r = 0$ is of considerable interest because it is the low value of $w_\infty(0)$ which requires the high peak values of w_∞ for the larger Re_r in order to effect the reduction of the radial mass flow to zero at $r = 0$. It was conjectured in Part I that $w_\infty(0)$ is the Bödewadt w_∞ based on the local angular velocity. The following simple analysis will show this conjecture, which is just an extension of Stewartson's conjecture for the $n = -1$ case, to be true within the framework of the present method.

For every Re_r there is a sufficiently small value of r such that

$$1 - \exp\left[-(1/2)\mathrm{Re}_r r^2\right] = \frac{1}{2}\,\mathrm{Re}_r r^2 \tag{3-31}$$

Consequently, for r smaller than this value, the Burgers' tangential velocity (Eq. 3-30) can be written

$$v_\infty = \omega r \tag{3-32}$$

where

$$\omega = \frac{1}{2}\,\frac{\mathrm{Re}_r}{1 - \exp\left[-(1/2)\mathrm{Re}_r\right]} \tag{3-33}$$

is the dimensionless angular velocity of the outer flow at $r = 0$. Since the circulation Γ_∞ is ωr^2, Eq. (2-31), the solution of the tangential momentum-integral equation, can be written

$$\tilde{\delta}^4 = \frac{1}{\omega^{\frac{4}{3}(1+B)}}\, r^{-\frac{8}{3}B}\left[\frac{1}{\omega^{\frac{2}{3}(1+B)}}\int_r^{r'} r^{-1+\frac{8}{3}B}\,dr + \int_{r'}^{1}\frac{r^{1/3}}{\Gamma_\infty^{\frac{2}{3}(1-2B)}}\,dr\right] \tag{3-34}$$

where r' is the value of r below which Eq. (3-32) is a valid approximation for v_∞. In the limit $r \to 0$, since $B < 0$,

$$\tilde{\delta}^4(0) = \left(-\frac{3}{8B}\right)\frac{1}{\omega^2} \tag{3-35}$$

The quantity $(-3/8B)$ is the Bödewadt solution in tilde form (Eq. 3-15). The definition of δ, from Eq. (2-3), can be written

$$\delta = \delta^*\,(\Omega_1^*/\nu^*)^{1/2} \tag{3-36}$$

where

$$\Omega_1^* = \frac{v_1^*}{r_1^*} \tag{3-37}$$

is the angular velocity of the outer flow at $r^* = r_1^*$, the edge of the disk. The relation between ω^*, the dimensional angular velocity at $r = 0$, and Ω_1^* is

$$\omega^* = \left(\frac{v_\infty^*}{r^*}\right)_{r=0} = \left(\frac{v_\infty}{r}\right)_{r=0}\frac{v_1^*}{r_1^*} = \omega\,\Omega_1^* \tag{3-38}$$

Therefore, if $\tilde{\delta}_\omega$ is the dimensionless $\tilde{\delta}$ based on ω^* instead of Ω_1^*, it follows from Eq. (3-35) that

$$\left[\tilde{\delta}_\omega(0)\right]^4 = \left[\tilde{\delta}^*(0)\right]^4\left(\frac{\omega^*}{\nu^*}\right)^2 = \left[\tilde{\delta}^*(0)\right]^4\left(\frac{\Omega_1^*}{\nu^*}\right)^2\omega^2 = \tilde{\delta}^4(0)\,\omega^2 = -\frac{3}{8B} \tag{3-39}$$

The Bödewadt value is obtained and the conjecture is proven. There is nothing in the preceding analysis which limits it to the Burgers' vortex. It applies to any tangential velocity distribution which has the behavior $v_\infty = \omega r$ near $r = 0$.

From Eqs. (2-34) and (3-35), the mass flow near $r = 0$ for $v_\infty = \omega r$ is

$$M = \left(-\frac{3}{8B}\right)^{3/4}\tilde{I}_1(\omega)^{1/2}\,r^2 \tag{3-40}$$

and, therefore, from Eq. (2-36),

$$w_\infty(0) = 2\left(-\frac{3}{8B}\right)^{3/4}\tilde{I}_1(\omega)^{1/2} \tag{3-41}$$

The values of w_∞ at $r = 0$ given in Fig. 8 agree with this formula.

If the Bödewadt velocity profiles are used in place of the Stewartson profiles, then, since $\bar{\delta}(0) = 1$ for $n = -1$ ($\omega = 1$), it follows from Eq. (3-35) that

$$\bar{\delta}(0) = \frac{1}{\omega^2} \tag{3-42}$$

for a velocity distribution with $v_\infty = \omega r$ near $r = 0$. It further follows from Eqs. (3-27) and (3-41) that

$$w_\infty(0) = 2\bar{I}_1(\omega)^{1/2} \tag{3-43}$$

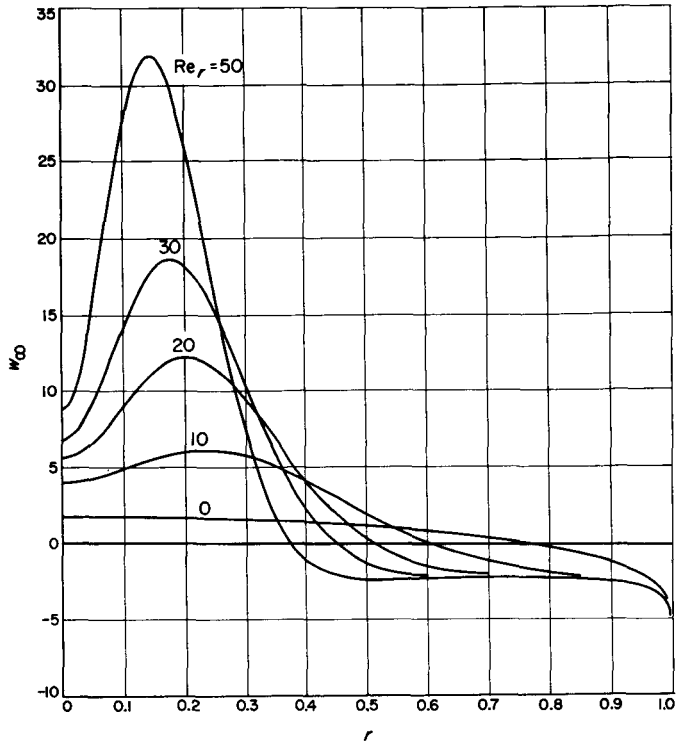

Fig. 8. Axial outflow velocity distribution for Burgers'-vortex outer flow. Stewartson velocity profiles

Consequently $w_\infty(0)$ is just the Bödewadt axial outflow velocity times $(\omega)^{1/2}$, a result that can also be derived directly from the definition of w in Eq. (2-3).

The axial outflow velocity distribution for the Bödewadt profiles is shown in Fig. 9 for $\mathrm{Re}_r = 20$. For comparison purposes, the distribution for the Stewartson profiles is repeated from Fig. 8. Just as in the $n = -1$ case, the exact w_∞ can be expected to lie along the Stewartson distribution near $r = 1$ and to shift gradually to the Bödewadt distribution as r decreases. In Fig. 10, the maximum w_∞ is shown as a function of Re_r for both profiles. Also shown is the exact value of $w_\infty(0)$, $1.35 \times (\omega)^{1/2}$, where ω is given by Eq. (3-33).

In Fig. 11 is shown the distribution with radius for a few Re_r of the maximum radial velocity in the boundary layer for the Stewartson velocity profiles. This quantity, from Eqs. (2-17) and (2-25), is given by

$$u_{max} = \frac{v_\infty^2}{r} \tilde{\delta}^2 [\tilde{f}(y)]_{max} \qquad (3\text{-}44)$$

The value of $[\tilde{f}(y)]_{max}$ is 0.620. A similar expression exists for the Bödewadt profiles in which bar quantities replace the tilde quantities. The value of $[\bar{f}(z)]_{max}$ is 0.484. Figure 12 is a companion plot to Fig. 10. It gives the peak value of u_{max} as a function of Re_r for both velocity profiles. The maximum value of v_∞ is also shown in Fig. 12.

A comparison of the magnitudes of the three velocity components is of interest because of the large values attained by w_∞ as Re_r increases. From Eq. (2-3), the ratio of the dimensional axial outflow velocity to the peripheral tangential velocity is dependent on Re_t. As an example, for $\mathrm{Re}_r = 100$ the ratio w_∞^*/v_1^* is 0.66 at $\mathrm{Re}_t = 10^4$ for the Stewartson profiles, and even larger for the Bödewadt profiles; at $\mathrm{Re}_t = 10^5$ it is 0.21. For the same Re_r, the peak values of v_∞ and u_{max} are 4.5 and 5.9, respectively, so these two quantities are of similar magnitude. The ratio of $(w_\infty^*)_{max}$ to $(v_\infty^*)_{max}$ is 0.15 at $\mathrm{Re}_t = 10^4$ and it becomes larger with increasing Re_r. As an extreme case, for $\mathrm{Re}_r = 5000$ ($\omega = 2500$) and $\mathrm{Re}_t = 10^4$, the ratio is 0.99. The ratio of $(w_\infty^*)_{max}$ to the local v_∞^* is only slightly larger, since the peak value of w_∞^* occurs near the peak of v_∞^*.

It is not known how large a value of ω can be produced at $r = 0$ over a surface in which there is no exit hole. If values of 100 and larger are possible, then the above analysis indicates a state of affairs not envisaged by the

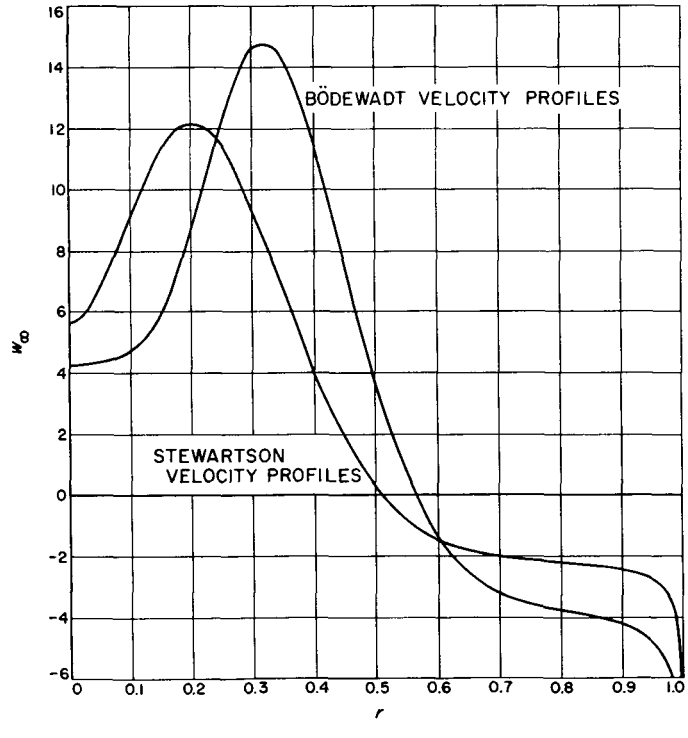

Fig. 9. Comparison of axial outflow velocity distribution for Burgers'-vortex outer flow with Stewartson and Bödewadt velocity profiles, $\mathrm{Re}_r = 20$

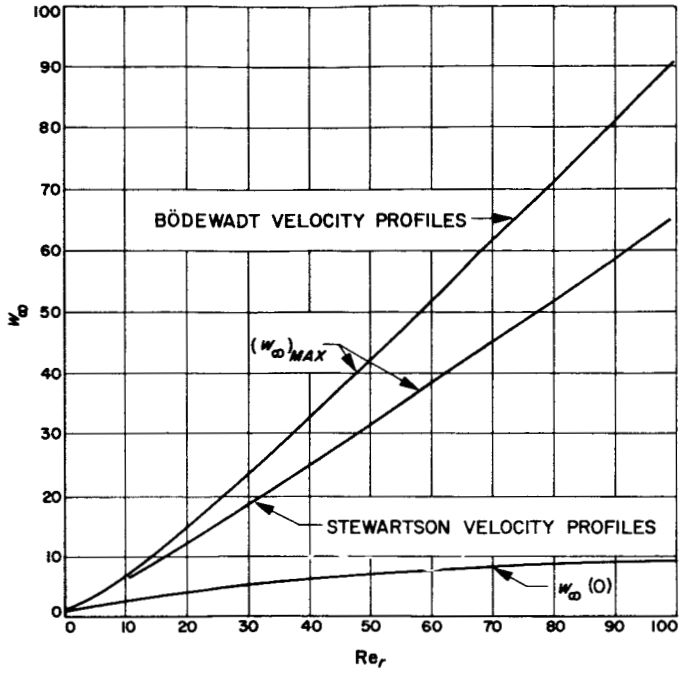

Fig. 10. Maximum axial outflow velocity for Stewartson and Bödewadt velocity profiles and exact axial outflow velocity at $r=0$ as functions of Re_r

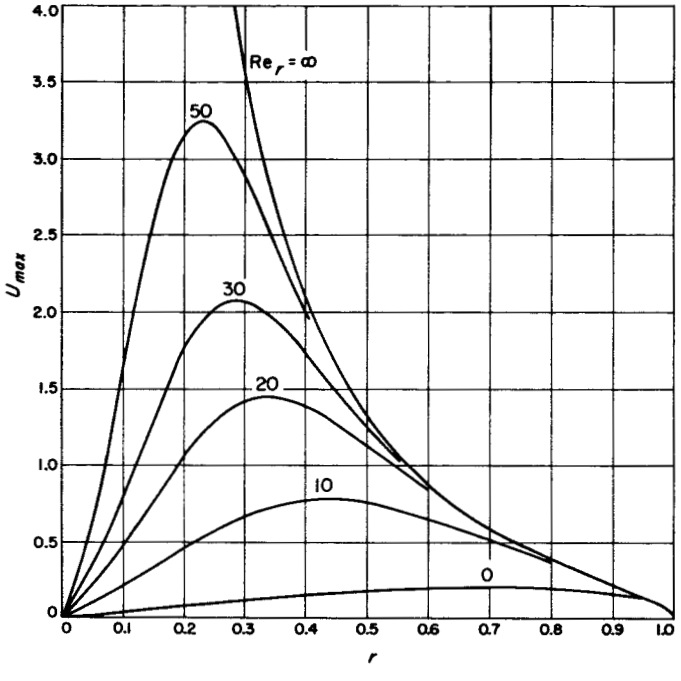

Fig. 11. Distribution with radius of maximum radial velocity in boundary layer. Stewartson velocity profiles

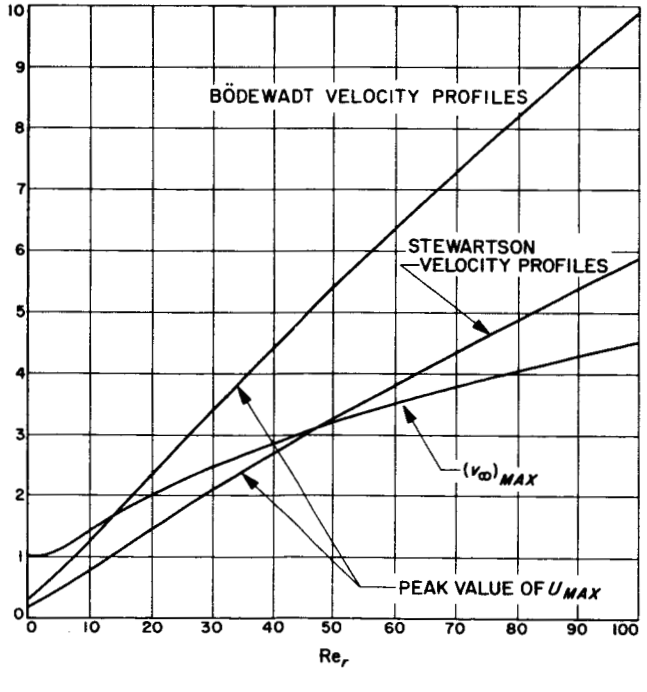

Fig. 12. Peak value of maximum radial velocity in boundary layer for Stewartson and Bödewadt velocity profiles and maximum value of v_∞ as functions of Re_r

boundary-layer theory, in which a fundamental assumption is that w^* is small compared to u^* and v^*. If the Bödewadt solution exists as a local solution near $r = 0$ under all circumstances, then the boundary-layer equations are valid there since they are also the Navier-Stokes equations under the Bödewadt similarity assumptions. Furthermore, they are also certainly valid some distance away from $r = 0$ where $w_\infty{}^*$ is small, but it is conceivable that an intermediate region can exist in which the flow is governed by some other equations.

NOMENCLATURE

A velocity-profile constant, Eq. (2-48)

B velocity-profile constant, Eq. (2-15)

C velocity-profile constant, Eq. (2-49)

D velocity-profile constant, Eq. (2-16)

$E(r)$ amplitude coefficient of radial velocity, Eq. (2-8)

$f(\eta)$ radial-velocity profile function, Eq. (2-8) [tilde form, Eq. (2-25); bar form, Eq. (3-26)]

$g(\eta)$ tangential-velocity profile function, Eq. (2-9) [tilde form, Eq. (2-26)]

I_1 integral of radial-velocity profile function [tilde form, Eq. (2-35); bar form, Eq. (3-24)]

$M(r)$ dimensionless inward radial mass flow in boundary layer, Eq. (2-33)

M_{max} maximum inward radial mass flow in boundary layer

n exponent of power law for outer-flow tangential velocity, Eq. (3-1)

r dimensionless radius, Eq. (2-3)

r_{max} radius of maximum radial mass flow in boundary layer

Re_r radial Reynolds number, a parameter in tangential velocity distribution of Burgers' vortex, Eq. (3-30)

Re_t peripheral tangential Reynolds number, Eq. (2-4)

$T(r)$ dimensionless torque, Eq. (2-42)

u dimensionless radial velocity, Eq. (2-3)

u_{max} maximum radial velocity in boundary layer at given radius, Eq. (3-44)

v dimensionless tangential velocity, Eq. (2-3)

v_∞ dimensionless tangential velocity of outer flow

w dimensionless axial velocity, Eq. (2-3)

w_∞ dimensionless axial outflow velocity

y Stewartson similarity variable, Eq. (2-21)

y_δ boundary-layer thickness in Stewartson variable

z dimensionless axial coordinate, Eq. (2-3)

Γ_∞ dimensionless circulation of outer flow, Eq. (2-19)

δ dimensionless boundary-layer thickness [tilde form, Eq. (2-29); bar form, Eq. (3-20)]

η boundary layer variable z/δ

θ angle between surface streamline and circumferential direction, Eq. (2-43)

ν^* kinematic viscosity coefficient

ρ^* density

τ_r dimensionless radial shear stress, Eq. (2-39)

τ_t dimensionless tangential shear stress, Eq. (2-40)

ω ratio of angular velocity of outer flow at $r = 0$ to angular velocity at $r = 1$

ω^* angular velocity of outer flow at $r = 0$

Ω_1^* angular velocity of outer flow at $r = 1$

Superscripts

* dimensional quantity

$\sim$ quantity in Stewartson formulation

$-$ quantity in Bödewadt formulation

Subscripts

1 reference quantity

∞ value at edge of boundary layer

B quantity as given by Bödewadt solution

REFERENCES

1. Mack, L. M., *The Laminar Boundary Layer on a Disk of Finite Radius in a Rotating Flow. Part I: Numerical Integration of the Momentum-Integral Equations and Application of the Results to the Flow in a Vortex Chamber,* Technical Report No. 32-224, Jet Propulsion Laboratory, Pasadena, May 1962.
2. von Kármán, T., "Über laminare und turbulente Reibung," *Zeitschrift für angewandte Mathematik und Mechanik,* Vol. 1, pp. 233-252, 1921.
3. Taylor, G. I., "The Boundary Layer in the Converging Nozzle of a Swirl Atomizer," *Quarterly Journal of Mechanics and Applied Mathematics,* Vol. 3, pp. 129-139, 1950.
4. Cooke, J. C., "On Pohlhausen's Method with Application to a Swirl Problem of Taylor," *Journal of the Aeronautical Sciences,* Vol. 19, pp. 486-490, 1952.
5. Mack, L. M., "The Laminar Boundary Layer on a Disk of Finite Radius in a Rotating Flow," Research Summary No. 36-14, pp. 103-105, Jet Propulsion Laboratory, Pasadena, 1962.
6. Stewartson, K., "On Rotating Laminar Boundary Layers," *Boundary Layer Research,* Symposium Freiburg (1957), pp. 59-71, Springer-Verlag, Berlin, 1958.
7. Bödewadt, U. T., "Die Drehströmung über festem Grunde," *Zeitschrift für angewandte Mathematik und Mechanik,* Vol. 20, pp. 241-253, 1940.
8. Cochran, W. G., "The Flow Due to a Rotating Disk," *Proceedings of the Cambridge Philosophical Society,* Vol. 30, pp. 365-375, 1934.
9. Burgers, J. M., "Application of a Model System to Illustrate Some Points of the Statistical Theory of Free Turbulence," *Proceedings of the Royal Academy of Sciences of Amsterdam,* Vol. 43, pp. 2-12, 1940.
10. Garbsch, K., "Über die Grenzschicht an der Wand eines Trichters mit innerer Wirbel- und Radialströmung," *50 Jahre Grenzschichtforschung,* Edited by H. Görtler and W. Tollmien, pp. 471-486, F. Vieweg, Braunschweig, 1955.
11. Browning, A. C., *Boundary Layer Theory* (Schlichting), p. 180, McGraw-Hill Book Co., New York, 1960.
12. Rogers, M. H., and G. N. Lance, "The Rotationally Symmetric Flow of a Viscous Fluid in the Presence of an Infinite Rotating Disk," *Journal of Fluid Mechanics,* Vol. 7, Part 4, pp. 617-631, April 1960.
13. Keyes, J. J., Jr., "Experimental Study of Flow and Separation in Vortex Tubes with Application to Gaseous Fission Heating," *ARS Journal,* Vol. 31, pp. 1204-1209, September 1961.